The clogging pressure of bubbles in hydrophilic microchannel contractions

Mads Jakob Jensen, Goran Goranović and Henrik Bruus

MIC—Department of Micro and Nanotechnology, Technical University of Denmark,
Oersteds Plads, Bldg. 345 East, DK-2800 Kgs. Lyngby, Denmark

E-mail: mjj@mic.dtu.dk

Abstract
We present a theoretical and numerical study of the quasi-static motion of
large wetting bubbles in microfluidic channels with contractions. In most
cases the energy of a bubble increases when it is moved from a wide channel
to a narrow one, and the bubble thus tends to clog the flow of the fluid. A
certain pressure, the so-called clogging pressure, is needed to push the
bubbles out of the contraction. However, we show that in the case of a
hydrophilic channel contraction there exists a range of parameter values
where the bubble actually gains energy by moving into the narrow part. For
these specific cases we analyze how the clogging pressure depends on
channel geometry, surface tension and contact angle. Based on our analysis
we establish design rules for minimizing the clogging pressure of
microchannel contractions.

1. Introduction

Many microfluidic networks on modern lab-on-a-chip devices
contain channel contractions. These tend to become
problematic if, as is often the case, gas bubbles are introduced
into the liquid at the inlets or by electrochemical processes.
Due to the small channel dimensions gas bubbles can easily
be large enough to span the entire channel cross-section.
Such 'large' bubbles are prone to get stuck at the channel
contraction, whereby they can clog the flow and disturb
measurements or functionality of the system in an uncontrolled
manner. To clear the clogged channel an external pressure,
the so-called clogging pressure, has to be applied to push
the clogging bubble out of the system. Although already
identified nearly a decade ago [1, 2], this important problem
in microfluidic systems has not been studied theoretically
to a wide extent, a situation we would like to amend with
this paper. The present work is a substantial extension of a
preliminary and specialized study presented at the NanoTech
2003 conference [3], now including an analysis of the bubble
energies in general cases, inclusion of compressibility effects
and the use of different parameter values.

A complete analysis of the motion of a large bubble
through a microchannel contraction involves many different
physical effects, some which are not completely understood.

Any comprehensive analysis would at least require detailed
modeling of the liquid–gas, liquid–solid and solid–gas
interfaces as well as the dynamics in the bulk fluids. But
also more complicated processes near the contact lines need
to be addressed, e.g. wetting [4–6], contact line pinning and
hysteresis [4, 7], dynamic contact angles and contact lines
[8–10] and static and dynamic friction [11–13]. It should be
stressed that many of these surface effects are hard to control
precisely, therefore dynamical systems where the lubrication
assumption is used are also widely analyzed [14, 15].

In this work, however, we will restrict our analysis to
quasi-static motion of bubbles. By this we mean that the
velocity of the bubble is nearly zero and that the entire
model system remains arbitrarily close to equilibrium for all
bubble positions. All dynamic aspects are thus neglected,
and basically the model involves only the free energy of the
internal interfaces of the system and external pressures. This
is motivated by the fact that it is difficult to experimentally
control surface related properties. We thus only study
geometry related effects. We also choose to work only with
axisymmetric channels of smooth (but otherwise arbitrary)
contraction geometries free from any sharp corners and
other singularities. With these simplifications the forces or
pressures needed to push a bubble through the system can be
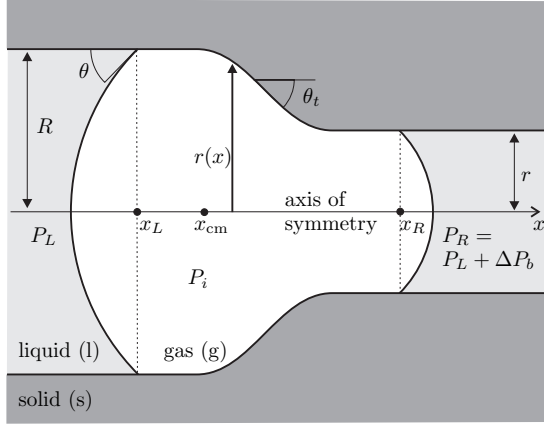calculated accurately without losing the essential physics of

Figure 1. A bubble with internal pressure P_i and center of mass x_{cm} in a hydrophilic axisymmetric channel. The left (right) contact line has the coordinate x_L (x_R) and contact angle θ. The channel is contracting from a straight part of radius R to one of radius r. The specific channel profile is defined by some function $r(x)$. Throughout this paper we have chosen $r(x)$ to be a sloped straight line joined to the straight parts by two circle arcs. The tapering angle θ_t is given by $\tan \theta_t = -r'(x)$. The pressure left (right) of the bubble is denoted as P_L (P_R) and the pressure difference across the bubble is ΔP_b.

the problem. This in turn enables us to formulate design rules for microchannel contractions to prevent or reduce clogging. To our knowledge similar analyses have only been made on channels of constant cross-sections [16] and for the special case of sudden contractions [17].

2. The model and basic physical assumptions

Consider a hydrophilic microfluidic channel or capillary, such as the one depicted in figure 1, which is axisymmetric about the x axis with a position dependent channel radius $r(x)$. The channel is filled with a liquid. A large bubble of some other fluid (we think mainly of a gas such as air) is present in the liquid. By large we mean that the volume of the bubble is larger than the volume V_{sph}^{max} of the largest inscribed sphere that can be placed anywhere in the microchannel. A large bubble divides the liquid into two disconnected parts, left and right of the bubble. The bubble itself consists of a bulk part in direct contact with the walls of the channel and of two menisci, in contact with the liquid, capping the ends of the bubble.

The bubble is assumed to be in quasi-static equilibrium. In that case it is relatively simple to combine mass conservation with geometric constraints to determine, as a function of the bubble position, the pressure drops over the two menisci needed to maintain this equilibrium. We define our central concept, the clogging pressure, as the maximum of the position dependent pressure drop across the bubble, i.e. the minimal external pressure that must be supplied to push the bubble through the microchannel.

2.1. The Young and Young–Laplace equations

Our model system consists of a solid channel containing a liquid and one large gas bubble. Therefore, the essential physical parameters are the three surface tensions (surface

free energy per area) σ_{lg}, σ_{sl} and σ_{sg} for the liquid–gas, solid–liquid and solid–gas interfaces, respectively. In equilibrium the contact angle θ is determined by the surface tensions through the Young equation [18, 19]

$$\sigma_{sg} - \sigma_{sl} = \sigma_{lg} \cos \theta. \tag{1}$$

In the following the contact angle is taken as the equilibrium angle or rather as an average contact angle. Because contact angle hysteresis is very sensitive to surface effects, we do not address these questions in this work.

To sustain a curved interface with the main radii of curvature R_1^c and R_2^c between a gas of pressure P_g and a liquid of pressure P_l, the pressure difference $\Delta P = P_g - P_l$ must obey the Young–Laplace equation [20]

$$\Delta P = \sigma_{lg} \left(\frac{1}{R_1^c} + \frac{1}{R_2^c} \right) = 2\sigma_{lg} \frac{\cos \theta}{r}, \tag{2}$$

where the last equation is applicable for a constant circular cross-section of radius r. We use the standard convention that these radii are taken as positive if the interface is concave when seen from the gas.

2.2. Isothermal motion and compressibility

In the rest of the paper we consider a 'large' bubble having the initial position '1' in the widest part of the channel. The initial volume is $V_1 = \gamma V_{sph}^{max}$, where $\gamma > 1$ and $V_{sph}^{max} = 4\pi r_1^3/3$, and the corresponding internal pressure is $P_{i,1}$. At a later stage the bubble is moved to a position '2', where the volume is V_2 and the internal pressure is $P_{i,2}$. In the quasi-static case the bubble motion is isothermal and hence the compressibility condition applies,

$$P_{i,1} V_1 = P_{i,2} V_2. \tag{3}$$

The pressure P_i within the bubble is given as the external pressure P_0 plus the pressure change ΔP across the curved interface, given by equation (2).

The most extreme compression is obtained by pressing a large bubble, which floats without geometrical constraints in a bulk liquid of pressure P_0, into a narrow circular channel of radius r. Combining equations (2) and (3) yields

$$\frac{V_1}{V_2} = \frac{P_{i,2}}{P_{i,1}} \approx \frac{P_{i,2}}{P_0} = 1 + \frac{2\sigma_{lg} \cos \theta}{r P_0}. \tag{4}$$

For example, moving a large spherical air bubble in water ($\sigma_{lg} = 0.0725 \, \text{J m}^{-2}$) at the ambient pressure $P_0 = 10^5 \, \text{Pa}$ into a channel of radius $r = 25 \, \mu\text{m}$ leads to $V_1/V_2 \approx 1.06$, i.e. a volume compression of 6%. Moving, as in section 6, a bubble from a 300 μm to a 190 μm wide channel yields a compression of about 0.2%.

In the case of laser ablated microchannels in plastic chips, compressibility effects are negligible as the smallest dimensions typically are greater than 100 μm. However, for silicon based micro- or nanofluidic devices, compressibility may play a significant role.

2.3. Quasi-static motion and geometry

For a bubble positioned in a microchannel contraction, the total internal energy E_{tot} is the sum of the surface free energy, gravitational energy, kinetic energy and frictional energy. We regard the surrounding pressures as external energy. By our definition quasi-static motion of an incompressible bubble

implies that the kinetic energy is zero and friction is also zero because of hydrostatic and thermodynamic equilibrium. Finally, we treat channels of characteristic dimensions $2r$ less than $300\,\mu\text{m}$, which is significantly smaller than the capillary length of water, $\Delta_c = \sqrt{\sigma_{\text{lg}}/\rho_{\text{l}} g} \approx 2700\,\mu\text{m}$, where $\rho_{\text{l}} = 10^3\,\text{kg m}^{-3}$ and $g = 9.82\,\text{m/s}^2$. So the gravitational energy can also be neglected, which ensures that the menisci may be approximated by spherical caps.

The total internal energy E_{tot} of the microchannel containing a quasi-statically moving bubble is given only by the surface free energy, i.e. the sum of interfacial energies σ_i times interfacial areas A_i,

$$E_{\text{tot}} = \sum_i \sigma_i A_i = \sigma_{\text{lg}} A_{\text{lg}} + \sigma_{\text{sg}} A_{\text{sg}} + \sigma_{\text{sl}} A_{\text{sl}}. \qquad (5)$$

The pressure-related applied external force F needed to balance the bubble is given by the gradient of the total internal energy with respect to the center of mass coordinate of the bubble x_{cm}. Hence

$$F = \frac{\text{d}E_{\text{tot}}}{\text{d}x_{\text{cm}}}, \qquad (6)$$

which thus depends on the bubble position x_{cm} and, through the areas A_i, on the geometry of the channel.

2.4. The clogging pressure

The Young–Laplace pressure drops (cf equation (2)) at the menisci are given by,

$$\Delta P_{\text{L}} = P_{\text{i}} - P_{\text{L}}, \qquad (7a)$$

$$\Delta P_{\text{R}} = P_{\text{i}} - P_{\text{R}}. \qquad (7b)$$

The total pressure drop $\Delta P_{\text{b}}(x_{\text{cm}})$ over the bubble as a function of its center of mass x_{cm} is given by

$$\Delta P_{\text{b}}(x_{\text{cm}}) = P_{\text{R}} - P_{\text{L}} = \Delta P_{\text{L}}(x_{\text{cm}}) - \Delta P_{\text{R}}(x_{\text{cm}}). \qquad (8)$$

The clogging pressure P_{clog} is defined as the maximal position dependent pressure drop across the bubble,

$$P_{\text{clog}} = \max\{-\Delta P_{\text{b}}(x_{\text{cm}})\}. \qquad (9)$$

The clogging pressure expresses the minimal amount by which the left-hand-side pressure P_{L} must exceed the right-hand-side pressure P_{R} to push the bubble through the contraction quasi-statically from left to right.

3. General energy considerations for axisymmetric microchannels

Consider a bubble placed in a cylindrical channel of radius R. We want to determine the change in energy resulting from moving it into a smaller channel of radius $r < R$, e.g. by moving it from left to right in the channel depicted in figure 1. Intuitively, we would expect the energy to increase as a result of the movement. In most cases this intuition is correct; however, we shall see that in some cases the system gains energy by the move, solely due to geometric conditions.

The bubble has the initial volume $V_1 = \gamma V_{\text{sph}}^{\text{max}}$, where $\gamma > 1$ and $V_{\text{sph}}^{\text{max}} = 4\pi R^3/3$. With this constraint the bubble is

forced to touch the walls regardless of its position. According to equations (2) and (7b) the internal pressure of the bubble is

$$P_{\text{i},1} = P_{\text{R}} + 2\sigma_{\text{lg}} \frac{\cos\theta}{R}. \qquad (10)$$

The volume of the bubble is the sum of two spherical cap volumes and the volume of a cylinder of initial length L. Once the length L is known, the relevant interfacial areas A_{lg} and A_{sg} may be found.

The gas bubble is now moved to the cylindrical channel of radius r, and according to equations (2), (3) and (7b) the pressure $P_{\text{i},2}$ and volume V_2 are

$$P_{\text{i},2} = P_{\text{R}} + 2\sigma_{\text{lg}} \frac{\cos\theta}{r}, \qquad (11)$$

$$V_2 = \frac{P_{\text{i},1}}{P_{\text{i},2}} V_1. \qquad (12)$$

By solving equation (12) it is straightforward to find the change in total free surface energy,

$$\Delta E_{\text{tot}} = E_{\text{tot},2} - E_{\text{tot},1} = \sigma_{\text{lg}}(A_{\text{lg},2} - A_{\text{lg},1}) + \sigma_{\text{lg}} 2\pi \cos\theta (rl - RL), \qquad (13)$$

where l is the length of the bubble in the channel of radius $r < R$ (situation 2). In equation (13) the Young relation (1) has been used to eliminate the solid–liquid and solid–gas interfacial energies.

Based on equation (13) we can analyze the energy change when moving the bubble from the wide channel of radius R to the narrow channel of radius r. First we give the limiting values of ΔE_{tot}. In the limit $r/R \to 1$ we obviously get $\Delta E_{\text{tot}} \to 0$. In the opposite limit, $r/R \to 0$, the compressibility of the bubble results in convergence of ΔE_{tot},

$$\lim_{\frac{r}{R} \to 0} \Delta E_{\text{tot}} = \frac{\pi R^3}{3} \left(4\gamma R P_{\text{R}} - \sigma_{\text{lg}} \frac{4 + \sin(3\theta) - 3\tan\theta}{\cos^2\theta}\right). \qquad (14)$$

To discuss ΔE_{tot} for general values of r/R we use a numerical example: an air bubble in a water filled PMMA channel for which we have the parameter values $P_{\text{R}} = 10^5\,\text{Pa}$, $\sigma_{\text{lg}} = 72.5\,\text{mJ}$ and $\theta = 72°$. The radius ratio r/R and the volume parameter γ are then varied.

In figure 2 the energy ΔE_{tot} (equation (13)) is plotted as a function of the ratio r/R for given values of γ. The figure shows that for large values of γ, i.e. large bubbles, it requires energy ($\Delta E_{\text{tot}} > 0$) to move the bubble from the wide to the narrow channel. However, there exists a critical value $\gamma_{\text{c}} \approx 4.75$ below which the system can gain energy by moving the bubble, if the radius ratio r/R is not too small. This behavior is generic for a bubble in a contracting channel, but the specific shape of the curve and the optimal minimum depend on the material parameters and the external pressure P_{R}.

The critical value γ_{c}, above which energy gain is impossible, is given by $\partial\Delta E_{\text{tot}}/\partial(r/R) = 0$ at $r/R = 1$,

$$\gamma_{\text{c}} = \frac{(3 - \cos(3\theta) + 2\sin\theta)(2\sigma_{\text{lg}}\cos\theta + R P_0)}{2R P_{\text{R}} \cos\theta(1 + \sin\theta)}. \qquad (15)$$

Figure 3 depicts the energy ΔE_{tot} as a function of the ratio r/R for $\gamma = 1$ and $\gamma = 3$, and for five values of the wide channel radius, $R = 100, 150, 200, 250$ and $300\,\mu\text{m}$.
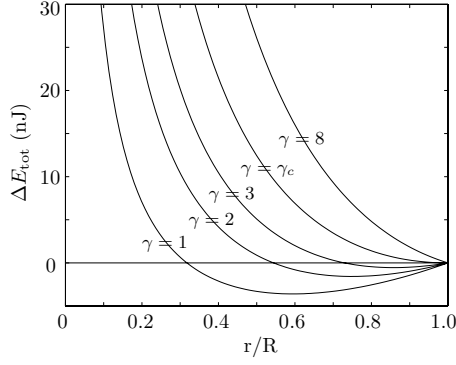
Figure 2. Plot of the energy change ΔE_{tot} as a function of the ratio r/R. The bubble is moved from a wide channel of radius $R = 150\,\mu\text{m}$ to a narrow channel of radius r. Five curves are shown corresponding to the volume ratio $\gamma = 1, 2, 3, \gamma_c$ and 8, respectively. $\gamma_c \approx 4.75$. For 'small' volumes $1 \leqslant \gamma < \gamma_c$ the system can gain energy by moving the bubble to the narrow channel, if the width of the latter is not too small. For $\gamma > \gamma_c$ the movement requires energy in all cases.
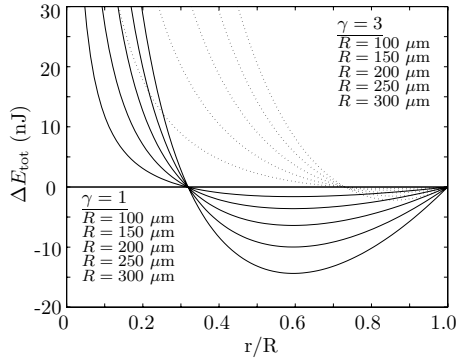

Figure 3. The energy ΔE_{tot} as a function of the ratio r/R for different values of the wide channel radius, $R = 100, 150, 200, 250$ and $300\,\mu\text{m}$. The plain curves correspond to the smallest bubble for $\gamma = 1$ and the dotted curves correspond to a larger bubble with $\gamma = 3$.

From equation (13) it may be seen that $\min\{\Delta E_{\text{tot}}\} \propto R^2$ as the area is proportional to R^2 and L is proportional to R. Deviations from this proportionality arise for small values of R because of compressibility. For $\gamma = 1$ in figure 3 we find $\max\{-\Delta E_{\text{tot}}\} = kR^2$ with $k = 0.159\,\text{J m}^{-2}$. This proportionality is illustrated as the energy at a given r/R point is increased by a factor 4 when R is doubled, e.g. from $R = 150\,\mu\text{m}$ to $R = 300\,\mu\text{m}$.

The previous calculations clearly show that for some geometries it is favorable to place the bubble in the narrow rather than in the wide part of the channel. In the following we shall address the question of whether for such geometries the bubble will move spontaneously or it must cross an energy barrier to arrive at the low-energy state in the narrow channel.

4. Analytical results for contractions with energy gain

Combining the geometry defined in figure 1 with equations (2) and (8), the central expression of our analysis is easily derived,
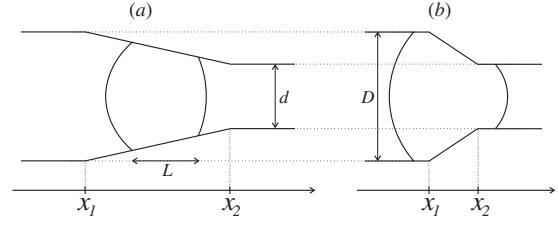

Figure 4. Two generic situations for a bubble of length $L = x_R - x_L$ near a microchannel contraction of length $x_2 - x_1$. (a) The contraction is long enough to contain the entire bubble, i.e. $x_R - x_L < x_2 - x_1$. (b) The contraction is so short that the bubble can span it completely, i.e. $x_R - x_L > x_2 - x_1$, which is a class β_4 bubble.

$$\Delta P_b = 2\sigma_{\text{lg}} \left(\frac{\cos[\theta - \theta_t(x_L)]}{r(x_L)} - \frac{\cos[\theta + \theta_t(x_R)]}{r(x_R)} \right). \quad (16)$$

From the discussion in section 2.4 it follows that if $\Delta P_b < 0$ then the contraction causes bubble clogging, whereas for $\Delta P_b > 0$ the bubble tends to move spontaneously through the contraction toward the narrow part.

Based on equation (16) a number of design rules may be established specifying the geometric features that may prevent or decrease clogging. Consider a bubble that starts out in the wide straight section left of the contraction, where it has a length $L_0 = x_R - x_L$. The pressure drop ΔP_b is zero to begin with, but depending on the shape of the contraction, such as the two examples shown in figure 4, ΔP_b changes as the bubble advances quasi-statically through the contraction.

The first part of any contraction can always be approximated by a circle with an arc angle which is the local tapering angle θ_t. As the right contact line x_R just enters the contraction, equation (16) can be expanded to first order in θ_t yielding

$$\Delta P_b \approx \frac{2\sigma_{\text{lg}} \sin \theta}{R} \theta_t > 0. \quad (17)$$

Thus initially the bubble tends to move spontaneously into the contraction. The physical reason for this is that the local tapering angle allows the meniscus to flatten a little, which reduces the costly gas–liquid interface energy.

Once the bubble moves inside the contraction defined in figure 1, a complicated interplay between the initial bubble length L_0, the contact angle θ, the channel radii $r(x_L)$ and $r(x_R)$ at the contact lines and the local tapering angle $\theta_t(x)$ decides whether bubble clogging occurs or not. We classify our systems into two main classes:

Class α comprises all cases where no clogging occurs, i.e. where the bubble can move spontaneously through the contraction without applying an external pressure.

Class β contains all cases with clogging, i.e. where $\Delta P_b < 0$ at some point or, equivalently, where $P_{\text{clog}} > 0$.

For class β four sub-classes can be identified depending on where the bubble is when ΔP_b becomes negative and clogging occurs. This bubble position is classified by the position of the contact lines x_L and x_R relative to the beginning x_1 and the end x_2 of the contraction region (see figures 1 and 4):

$$\begin{aligned}
\text{class } \beta_1: & & x_L < x_1 & \text{ and } & x_1 < x_R < x_2, \\
\text{class } \beta_2: & x_1 < x_L < x_2 & \text{ and } & x_1 < x_R < x_2, \\
\text{class } \beta_3: & x_1 < x_L < x_2 & \text{ and } & x_2 < x_R, \\
\text{class } \beta_4: & & x_L < x_1 & \text{ and } & x_2 < x_R.
\end{aligned} \quad (18)$$

Table 1. Physical parameters for air bubbles in water flowing through PMMA microchannels.

Parameter values	Reference
$\sigma_{lg} = 72.5 \times 10^{-3} \text{ J m}^{-2}$	[21]
$\sigma_{sg} = 38.9 \times 10^{-3} \text{ J m}^{-2}$	[21]
$\sigma_{sl} = 16.5 \times 10^{-3} \text{ J m}^{-2}$	[21]
$\theta = 72°$	[18]

A detailed analysis of equation (16) yields important relations for some of the clogging classes.

A β_2 clogging only occurs if the bubble can move entirely within the tapered region as shown in figure 4(*a*), and if at some point it has a length $L = x_L - x_R$ such that

$$L > \frac{r(x_L)}{\tan \theta_t} \left[1 - \frac{\cos(\theta - \theta_t)}{\cos(\theta + \theta_t)} \right]. \qquad (19)$$

In β_4 where the bubble in fact spans the entire contraction as sketched in figure 4(*b*), there is always clogging and the clogging pressure is maximal. The value for ΔP_b is negative and independent of the shape of the contraction. From equation (16) we get

$$\Delta P_b = 2\sigma_{lg} \cos \theta \left(\frac{1}{R} - \frac{1}{r} \right) < 0. \qquad (20)$$

The nonclogging class α will in general occur if the bubble is small enough. According to the class β_4 analysis a necessary (but not sufficient) condition for avoiding clogging is that the bubble is small enough to be completely contained in the contraction region. An analysis of the β_2 and β_3 classes shows that it should also be short enough to avoid clogging while the left meniscus is still in the tapered region. The β_1 class furthermore puts upper limits on tapering angles that allow for clog-free flow. Examples from class α and β_4 are treated further by detailed numerical analysis in sections 5.2 and 5.3.

5. Numerical simulations

To illustrate the analysis given above a detailed simulation is made in the following. The aim is to minimize the clogging pressure ΔP_b with respect to a given parameter. We are limiting our analysis so that the variation comprises only one parameter: the tapering angle θ_t.

5.1. The numerical algorithm

In order to find the force and clogging pressure acting on a large bubble for a given geometry, a semianalytical model of the contracting channel is implemented in MatLab. A numerical Romberg integration scheme is used together with a Newton solver to determine the location of the right and left contacts line (x_R and x_L) for a given position of the center of mass coordinate x_{cm}. The respective interface areas A_i are then found. For a specific geometry defined through $r(x)$, the maximal force is found through equations (5) and (6) and the pressure drop ΔP_b is found through equation (16). The heaviest calculation ran for approximately 4 h on a standard PC.

To be specific we use the geometry defined in figure 1 and take PMMA as the solid material, water as the liquid and air as the gas. This configuration has the physical parameters given in table 1.

5.2. A specific system without clogging, class α

The first example is the system with a bubble placed in a relatively gentle contraction depicted in figure 5. The total length of the channel is 1000 μm. The wide straight channel to the left has a radius $R = 150 \ \mu$m and length 200 μm. The contraction has a length $x_2 - x_1 = 350 \ \mu$m and circle arc lengths of 30 μm, which results in a tapering angle $\theta_t = 10°$. The narrow straight channel to the left has a radius $r = 95 \ \mu$m and length 500 μm. The bubble starts out in the wide channel to the left. It has a relative volume of $\gamma = 1.02$ (cf section 3) and an initial length $L_0 = 180 \ \mu$m.

Figure 5 shows the bubble at five different positions (*a*)–(*e*). As the bubble advances through the channel it is seen how its length $x_R - x_L$ changes and how the curvatures of the menisci vary. The black dots inside the bubble indicate the center of mass x_{cm}.

In figure 6(*a*) the total internal energy of the system is plotted as a function of center of mass position x_{cm}. The zero point of the energy is chosen as the energy of the system when the entire bubble is positioned completely within the narrow part of the channel. The five positions (*a*)–(*e*) in figure 5 are also marked here.

It is seen that the energy decreases monotonically. This means that without a negative external pressure holding it back, it would move spontaneously through the channel from the left to the right. As long as the bubble moves completely within the wide part of the channel, the energy is constant (about 4 nJ). Then as the right edge enters the contraction, position (*a*), the energy drops rapidly in accordance with the pressure drop equation (17). This trend continues as the entire bubble moves inside the contraction, as is the case in position (*b*). The energy continues to drop, but now less rapidly, as the right edge of the bubble enters the narrow channel, see position (*c*). However, as the left bubble edge approaches the narrow channel, the energy drop picks up again, see position (*d*). Finally, the bubble moves completely inside the narrow section and the energy becomes zero (per definition), see position (*e*).

In figure 6(*b*) the corresponding balancing external force F from equation (6), and the clogging pressure across the bubble $-\Delta P_b$, equation (16), are plotted as functions of x_{cm}. The balancing external force is seen to be negative, which means that to maintain the bubble at quasi-static equilibrium, it is necessary to hold it back. Without this force, the bubble would of course, as mentioned above, move spontaneously toward the narrow segment. At position (*c*) where the right edge of the bubble enters the narrow channel, both force and pressure reach local maxima, but even here they are both negative. No clogging occurs in this system, and it therefore belongs to class α as defined in section 4.

5.3. A specific channel with clogging, class β_4

The second example is nearly the same as the first. Only the length of the contraction region has been reduced from 350 μm to 180 μm. This leads to an increase of the tapering angle from 10° to $\theta_t = 20°$. In figure 7 four positions (*a*)–(*d*) of the large bubble are depicted. Note that since $\theta + \theta_t = 92°$, the right meniscus in the tapered section of the channel in panel (*a*) is nearly flat. In fact it has a slight inward bend.
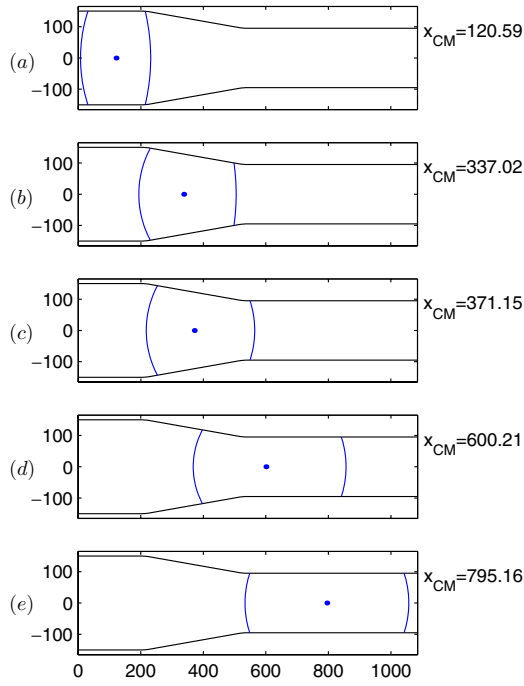
Figure 5. Five positions (a)–(e) of a large bubble with $\gamma = 1.02$ inside a 1000 μm long hydrophilic channel with a tapering angle $\theta_t = 10°$. The black dots indicate x_{cm}. The contact angle is $\theta = 72°$.

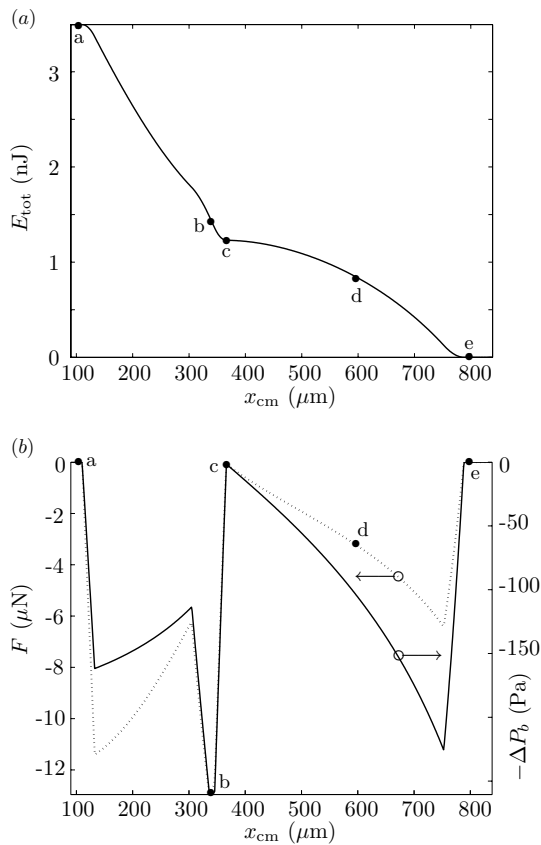**Figure 7.** Four positions (a)–(d) of a bubble with $\gamma = 1.02$ inside a 1000 μm long hydrophilic channel with the tapering angle $\theta_t = 20°$. The black dots indicate x_{cm}. The contact angle is $\theta = 72°$.

Figure 6. (a) A plot of the total internal energy E_{tot} versus the center of mass coordinate x_{cm} for the same bubble as in figure 5. (b) The balancing external force F and the pressure drop across the bubble ΔP_b versus x_{cm}. The five dots correspond to the five bubble positions in figure 5. Note that $-\Delta P_b < 0$ for all positions, i.e. no clogging occurs (a class α system).
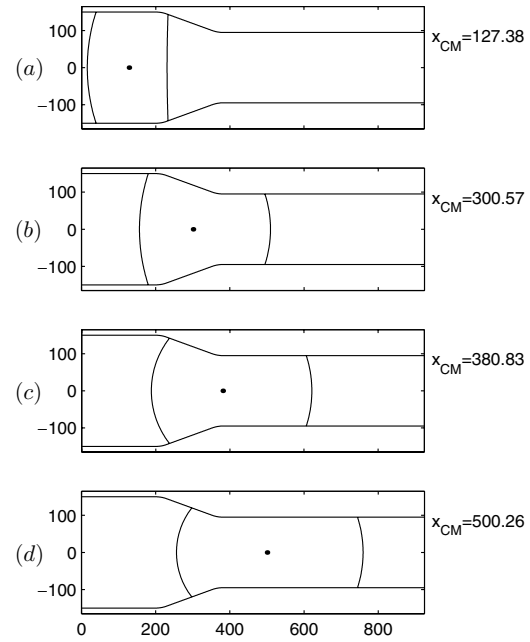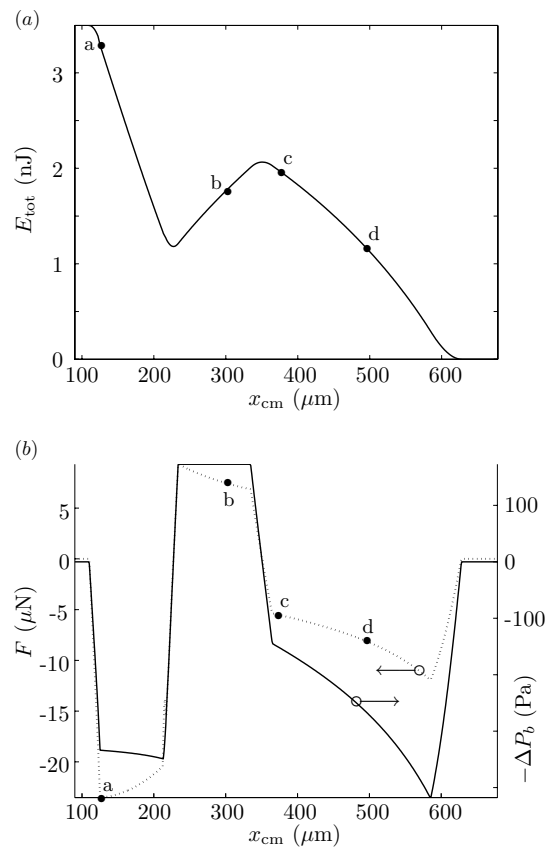
Figure 8. (a) A plot of the total internal energy E_{tot} versus the center of mass coordinate x_{cm} for the same bubble as in figure 7. (b) The balancing external force F and the pressure drop across the bubble ΔP_b versus x_{cm}. The four dots correspond to the four bubble positions in figure 7. Note that $-\Delta P_b > 0$ for x_{cm} around 300 μm, i.e. clogging occurs (a class β system).
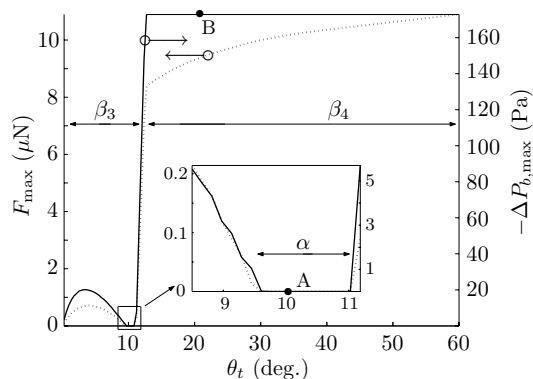
Figure 9. The maximal balancing force F_{max} and clogging pressure $P_{clog} = -\Delta P_{b,max}$ plotted as functions of the tapering angle θ_t. Detailed figures illustrating the situation for $\theta_t = 10°$ (marked A) are given in figures 6(*a*) and (*b*), and for $\theta_t = 20°$ (marked B) in figures 8(*a*) and (*b*). The β_3, β_4 and α classes are described in section 4. The maximal clogging pressure occurs in class β_4. It is found by equation (20) to be $P_{clog} = 173$ Pa.

In figure 8(*a*) the energy is shown as a function of x_{cm}. The four positions (*a*)–(*d*) are also marked. We immediately note a qualitative difference between this graph and that in figure 6(*a*). The energy no longer drops monotonically but exhibits a marked increase between positions (*b*) and (*c*). This corresponds to the case where the bubble spans the entire contraction, i.e. the left bubble edge is still in the wide channel segment when the right edge enters the narrow segment.

This effect is of course also visible in figure 8(*b*) where the balancing external force F and the clogging pressure $-\Delta P_b$ are plotted as functions of x_{cm}. Around position (*b*) both F and $-\Delta P_b$ become positive, which means that external pressure forces need to be applied to move the bubble through the system. Using equation (20) the clogging pressure is found to be 173 Pa. Without this external force the bubble would tend to move backwards out of the channel, i.e. the system is clogging, and in fact it is an example of class β_4 clogging.

5.4. Clogging pressure versus tapering angle θ_t

The previous two examples showed the behavior for a particular channel contraction from $R = 150\,\mu m$ to $r = 95\,\mu m$ with tapering angles $\theta_t = 10°$ and $20°$, respectively. We now extend this analysis to the entire interval $0° < \theta_t < 60°$. For each tapering angle we calculate the maximal external force F and the clogging pressure P_{clog}. The result is shown in figure 9.

The graph clearly shows that some tapering angles ease the passage of bubbles. For the geometrical configuration defined by $R = 150\,\mu m$, $r = 95\,\mu m$ and $C = 30\,\mu m$ a small window, the interval $9.5° < \theta_t < 11°$, with optimal tapering angles can be identified. In this window $P_{clog} < 0$ corresponding to the clogging-free class α behavior.

For angles greater than about $11°$ the maximal force is seen to increase dramatically. This transition corresponds to a configuration where the bubble can span the entire contraction region, i.e. class β_4. We clearly see that once the bubble is able to span the entire contraction, the specific geometry of

the contraction (in this case the tapering angle) plays no role. We get the same clogging pressure, $P_{clog} = 173$ Pa.

Finally, we note, that class β_3 behavior sets in for small tapering angles below $9.5°$. A small clogging pressure is observed, less than 30 Pa.

6. Conclusion

The effects of geometry on the quasi-static motion of large bubbles through a hydrophilic microchannel (capillary) contraction are modeled. The simplicity of the model leads to a good physical understanding of bubble clogging. We have shown that in most cases it requires energy to move a bubble from a wide to a narrow channel. However, we have also found that certain bubble sizes and specific channel geometries lead to a gain in energy.

We have specifically studied the contractions where such an energy gain is achieved. Using the central equation for the pressure drop ΔP_b across the bubble, equation (16), we analyzed a specific contracting axisymmetric hydrophilic channel, and we identified four different classes, denoted as β_1 to β_4, leading to bubble clogging, and one clogging-free class denoted as α. The details of the analysis are quite complicated due to the large number of parameters: the tapering angle θ_t, the contact angle θ, the initial bubble length L_0, the radii R and r of the wide and narrow channel segments, etc. However, one general trend is clear. The tendency for clogging increases as the bubbles become larger.

Based on our analysis, some important design rules can be established for making microchannel contractions with minimal or even vanishing clogging pressures. These rules only apply for channel contractions where the energy is lowest in the narrow part.

First, if the typical size L_0 of the bubbles present in the microfluidic system is known, it is important to design contractions which are larger than L_0. The highest clogging pressures occur namely for bubbles spanning the entire contraction, the so-called β_4 class.

Second, the combined effect of the tapering angle and contact angle has to be taken into account to make sure that L_0 is shorter than the critical length leading to clogging of class β_2 being entirely within the tapered region.

Third (not presented here), to smoothen out and lower any unavoidable positive clogging pressure, it helps to make the curved parts of the contraction as large as possible, thus decreasing their curvature.

The method of analyzing the bubble clogging problem in microchannels presented in this paper is very general. It is straightforward to extend it to other geometries (such as nonmonotonic contractions) and to hydrophobic microchannels. With the presented design rules at hand it is possible to design a system that may filter or sort bubbles of different volumes—one simply places contractions with different tapering angles in properly arranged series. A comparable system designed to sort bubbles is presented in [17]. The model may also be extended to include wetting layers as used in [16], and it may be used to model two phase flows in porous media as in [22, 23]. Some of the dynamical effects such as those briefly mentioned in the introduction may be included as well.

Acknowledgments

References

[1] Gravesen P, Branebjerg J and Søndergård Jensen O 1993 *J. Micromech. Microeng.* **3** 168

[2] Elwenspoek M, Kannerubj T S, Miyake R and Fluitman J H J 1994 *J. Micromech. Microeng.* **4** 227

[3] Jensen M J, Goranović G and Bruus H 2003 *Proc. NanoTech 2003 (San Francisco, USA, Feb. 2003)* vol 1 258–61

[4] de Gennes P G 1985 *Rev. Mod. Phys.* **57** 827

[5] Brochard-Wyart F and de Gennes P G 1992 *Adv. Colloid Interface Sci.* **39** 1

[6] Stoev K, Ramé E, Leonhardt T and Garoff S 1998 *Phys. Fluids* **10** 1793

[7] Raphaël E and de Gennes P G 1989 *J. Chem. Phys.* **90** 7577

[8] Dussan E B, Ramé V E and Garoff S 1991 *J. Fluid Mech.* **230** 97

[9] de Gennes P G, Hua X and Levinson P 1990 *J. Fluid Mech.* **212** 55

[10] Pismen L M and Rubinstein B Y 2001 *Langmuir* **17** 5265

[11] Tenan M A, Hackwood S and Beni G 1982 *J. Appl. Phys.* **53** 6687

[12] Parlange J-Y 1983 *J. Appl. Phys.* **54** 6744

[13] Schwartz A M, Rader C A and Huey E 1964 *Adv. Chem. Ser.* vol 43 ed R F Gould (Washington, DC: American Chemical Society) p 250

[14] Bretherton F P 1961 *J. Fluid Mech.* **10** 97

[15] Ratulowski J and Chang H -C 1989 *Phys. Fluids* A **1** 97

[16] Bico J and Quéré D 2002 *J. Fluid Mech.* **467** 101

[17] Tordeux C and Fournier J -B 2002 *Europhys. Lett.* **60** 875

[18] Adamson A W and Gast A P 1997 *Physical Chemistry of Surfaces* 6th edn (New York: Wiley)

[19] Probstein R F 1994 *Physiochemical Hydrodynamics: An Introduction* 2nd edn (New York: Wiley)

[20] Batchelor G K 2000 *An Introduction to Fluid Dynamics* (Cambridge: Cambridge University Press)

[21] Jańczuk B, Bialopiotrowicz T and Zdziennicka A 1999 *J. Colloid Interface Sci.* **211** 96

[22] Zha F F, Fane A G, Fall C J D and Schofield R W 1992 *J. Membr. Sci.* **75** 69

[23] Bear J 1998 *Dynamics of Fluids in Porous Media* (New York: Dover)